Ab Initio Study of the Lowest Energy Conformers and IR Spectra of Poly(amidoamine)-G0 Dendrimers

Francisco Tarazona-Vasquez and Perla B. Balbuena*

Department of Chemical Engineering, University of South Carolina, Columbia, South Carolina 29208

Received: February 14, 2004; In Final Form: May 23, 2004

A systematic sequential procedure is implemented to find local minimum conformers corresponding to the lowest generation (G0), $-NH_2$- and −OH-terminated, poly(amidoamine) (PAMAM) dendrimers, and their IR vibrational spectra using ab initio (Hartree−Fock and density functional theory) techniques. It is found that the most stable conformations of PAMAM-G0 dendrimers in the gas phase have all their secondary amide groups in the *trans* conformation. Interbranch interactions including intramolecular H-bonds play a definite role in providing structural stability. The calculated electronic density spatial distribution reveals the existence of three regions where appropriate environments would attract either an ion or a metal atom: the core, the amide, and the terminal group (NH_2 or OH) sites. A detailed analysis of the IR spectra for the lowest energy conformers of PAMAM-NH_2 and PAMAM-OH is thoroughly analyzed and compared with experimental data when available.

Introduction

Dendrimers are synthetic macromolecules which possess a tree-like, highly branched structure.[1−4] They consist of a core surrounded by symmetric branched structures, as shown in Chart 1 for the poly(amidoamine) (PAMAM) of the lowest generation, G0. The next generation, PAMAM-G1, is grown when each of the terminal Y atoms (Chart 1) is substituted by two identical branches such as those emerging from the core tertiary amines. The same procedure spawns higher order generations (PAMAM-G*n* dendrimers), which tend to adopt a spherical structure as the molecular weight increases.[5] Because of their peculiar chemical and geometrical structure that originate their dendritic encapsulation properties, dendrimers have recently generated a great deal of attention, for applications ranging from controlled fabrication of nanocatalysts to electronic devices with specific functions that take advantage of their energy-harvesting and light-emitting properties.[1,2,5−15]

Even though they possess a more flexible and open structure, low-generation dendrimers are also used as templating agents which provide peripheral reactive sites.[16] Additionally, because of their intrinsic nature, a sequential study of dendrimers starting from the lowest generations may provide valuable details about the mechanisms of ion and metal attachment to the dendrimer sites.[17−19] Experimental investigations using mass spectrometry,[20] electron paramagnetic resonance,[21,22] UV and visible absorption spectroscopy,[10] and NMR methods,[23] among others, have provided useful insights about ion and metal atom complexation. Theoretical and computational studies include classical molecular dynamics (MD)[24−27] as well as coarse-grained methods[28,29] which are mostly directed toward determining structural and dynamical aspects of high order generation dendrimers (usually G4 and higher) and their intermolecular interactions in solution, whereas only a few quantum density functional theory (DFT) studies have addressed structural and electronic aspects of low-generation dendrimers,[30] which can provide substantial information about the chemical and electronic nature of the adsorption sites.

CHART 1

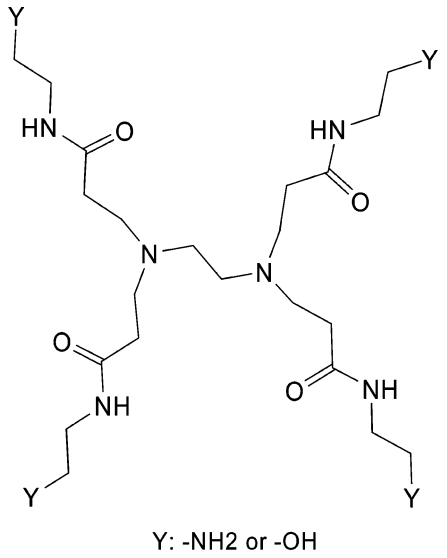

On the other hand, published experimental or theoretical studies of IR spectra are scarce, and they are restricted to a small spectral region.[31,32] Approaches that have been followed to calculate the IR spectra of dendrimers include summation of the absorption curves of the fragments under assumption of negligible interaction between terminal groups and the periodic part of the dendrimers.[18] A more strict approach is the normal-mode analysis of the molecules of low-generation dendrimers as shown for the IR spectra of the first generation of a phosphorus-containing starburst dendrimer by Furer et al.[17] However, it is not possible to apply normal-mode analysis beyond low-generation dendrimers. An alternative approach is based on the theory developed for calculation of the IR spectra of linear polymers.[17] In addition, recent theoretical reports[17,18,33]

* Corresponding author. Current address: Chemical Engineering Department, Texas A&M University, College Station, TX, 77843. E-mail: balbuena@tamu.edu.

10.1021/jp049325i CCC: $27.50
Published on Web 09/15/2004

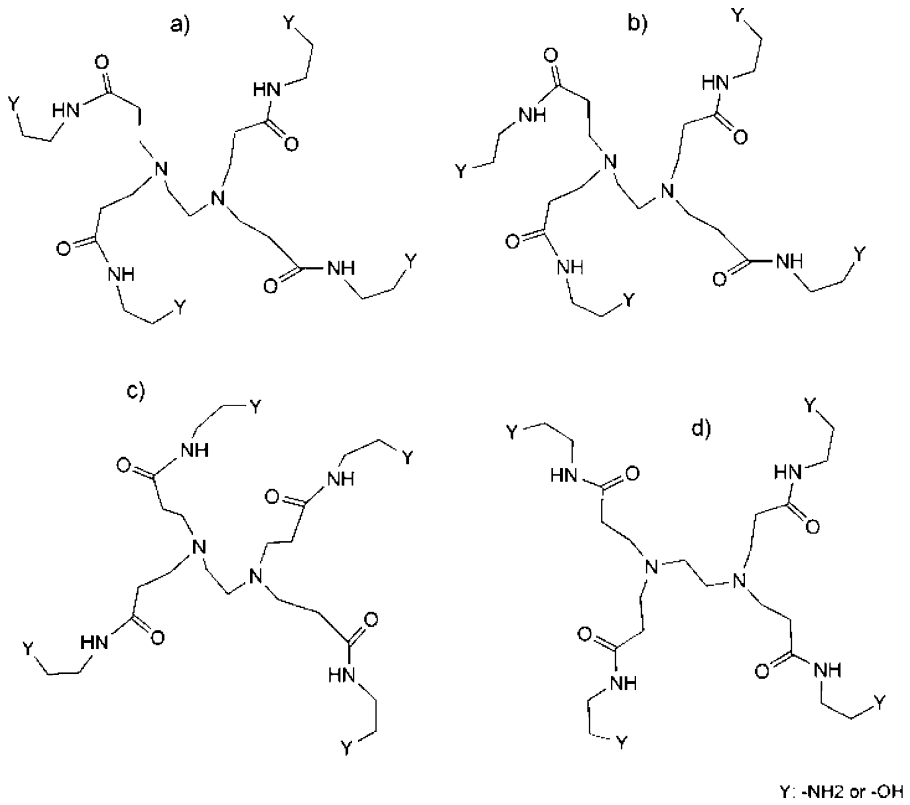

Figure 1. Schematic of G0 conformers: (a) *tttc*, (b) *tttt1*, (c) *tttt2*, (d) *tttt3*. In this representation it is possible to observe that the structural conformations of *tttc* and *tttt1* are nearly the same except for the *cis* vs *trans* position of one of their amide functional groups. The first three conformers have a NCCN core dihedral angle of approximately 60°, whereas in *tttt3* the dihedral value is 180°. In *tttt2* an intermolecular −NH···O hydrogen bond is noticeable.

indicate that the vibrational features found in G0 are basically repeated in the spectra of higher generation dendrimers. For large molecules, accurate predictions of harmonic frequencies and intensities from quantum mechanical calculations are important especially in the region below 1700 cm^{-1}, where the high density of states results in spectral complexity.[34]

We report a systematic ab initio investigation of the lowest generation PAMAM-G0 dendrimers (Chart 1) which initiates a series of studies tending to elucidate aspects of ion and metal complexation in solution. Our analysis focuses on the structure of the PAMAM-G0 lowest energy conformers in a vacuum, and includes the first complete description of the IR vibrational spectra for G0-NH_2 and G0-OH.

Methodology

The application of quantum chemical calculations to macromolecules[35] has benefited from significant advances in computer hardware and software. The intrinsic structural nature of dendrimers provides an additional advantage: the analyses of fragments and low-generation dendrimers allow the application of systematic procedures where building blocks are added sequentially, emulating the experimental synthesis methodologies.[2] Here we use a systematic sequential procedure for building and optimizing a PAMAM-G0-NH_2 (ethylenediamine, EDA, core). Initial optimizations were performed at the Hartree−Fock (HF) level of theory and the most basic STO-3G basis set for an EDA molecule. Then, one by one, branches were added by replacing the four amine-terminal hydrogen atoms and the resulting systems optimized until the optimized complete dendrimer structure was obtained. Successive steps involved improving the basis set (HF/3-21G, HF-6-31G(d), and HF/6-311G(d)) and incorporating electron correlation through DFT methods (B3LYP/6-311G(d)) to properly describe the electronic characteristics of various conformers and their IR vibrational spectra for both G0-NH_2 and G0-OH. Because one of our goals is to use the information obtained from these ab initio studies to parametrize effective force fields for molecular dynamics simulations, we carefully analyze the geometry and Mulliken population charges[36−38] of various local minimum conformers. All the calculations were performed using the Gaussian98 program.[39]

Results and Discussion

Search for Minimum Energy Conformers of G0-NH_2 and G0-OH. Full optimizations yielded two types of conformers: one where the secondary amide group of one of the branches is in the *cis* conformation, whereas all the others are in the *trans* position (*tttc*), and a second type where the four secondary amide groups are in the *trans* position, designated as *tttt1*, *tttt2*, and *tttt3* conformers (Figure 1).

Intramolecular interactions depend on the conformer structures: in G0-NH_2, both *tttt1* and *tttc* may form H-bonds between an H atom of one terminal primary amine and the amide O of an adjacent branch, whereas *tttt2*, which adopts a more extended and symmetric geometry than *tttt1*, only forms an H-bond between an amide O and an amide H of adjacent branches (Figure 1). Finally, we found another conformer, *tttt3* (Figure 1), which has three of its branches approximately coplanar, and the fourth slightly out of this plane, along with a core dihedral angle NCCN of about 180°. In G0-OH, *tttt2* may have H-bonding similar to that of its analogous G0-NH_2, whereas *tttt1* and *tttc* may form H-bonds between a H from a OH terminal group and an amide O of adjacent branches. The relative energies shown in Table 1 suggest that in a vacuum both dendrimers prefer to adopt the *all-trans* conformation.

TABLE 1: Full Optimizations (No Restrictions Imposed on the Symmetry in Either Geometry) of PAMAM Conformers at Various Levels of Theory[a]

		HF/6-31G(d)		B3LYP/6-31G(d)//HF/6-31G(d)	
PAMAM	conformer	energy (au)	rel energy[b]	energy (au)	rel energy[b]
G0-NH_2	tttc	−1704.26357	6.31	−1714.92559	3.47
	tttt1	−1704.26948	2.60	−1714.93112	0.00
	tttt2	−1704.26684	4.25	−1714.92386	4.56
	tttt3	−1704.27362	0.00	−1704.27362	5.21
G0-OH	tttc	−1783.60323	18.76	−1794.43207	3.52
	tttt1	−1783.63313	0.00	−1794.43768	0.00
	tttt2	−1783.60349	18.59	−1794.42168	10.04
	tttt3	−1783.62879	2.72	−1794.42123	10.32

[a] Corresponding schematic geometries are shown in Figure 1. [b] Relative energies in kilocalories per mole, referred to the lowest energy conformer for each set of conformers within the same method.

A substantial energy difference was found (Table 1) between *tttc* and *tttt* conformers. Table 1 indicates that, for G0-NH_2, the lowest energy conformer at HF/6-31G(d) is *tttt3*, with a small difference of 2.6 kcal/mol higher energy for *tttt1*. However, this difference reverts when electron correlation is introduced; thus, B3LYP/6-31G(d)//HF/6-31G(d) yields *tttt1* as the most stable conformer. The stability order between *tttt2* and *ttttc* also reverts when electron correlation is included, which may be due to the above-mentioned H-bonding ability of *tttt1* and *tttc*, which should be better described at the B3LYP/6-31G(d)//HF/6-31G-(d) level. A different behavior is found for G0-OH, where the calculated lowest energy conformer is *tttt1* regardless of the method used. At the HF/6-31G(d) level, the *tttt2* conformer is slightly less stable than *tttc*, and both have much higher energy than *tttt1* and *tttt3*, but at B3LYP/6-31-G(d)//HF/6-31G(d) the *tttt3* conformer is much less stable. Thus, these results suggest an important role of intramolecular hydrogen bonds in the stabilization and conformation of dendrimers. The relatively higher stability of *tttt1* compared with the corresponding *tttc* conformer is in agreement with the known preference for the amide *trans* over amide *cis* in protein backbones, and it is because of reduced steric hindrance. Moreover, the difference in energy, calculated including the correlation effect through DFT, between the G0 conformers *tttt1* and *tttc* is of the same order of magnitude found for the *trans*−*cis* isomerization in the gas phase of the peptide-bond-containing analogue *N*-methylacetamide.[40] It should be noticed that here we compare only *tttt1* and *tttc* conformers because of their apparent similarities that can be observed in Figure 1. The *tttt2* conformers are 4.56 and 10.4 kcal/mol less stable compared to *tttc* for G0-NH_2 and G0-OH, respectively, suggesting the importance of the intramolecular hydrogen bond interactions in stabilizing the conformers. This difference may be explained on the basis of the existence of at least two H-bond interactions in *tttc* and *tttt1*, whereas only one is present in the *tttt2* conformers.

Another factor that contributes to the stability of G0 conformers is the value of the core dihedral angle NCCN. HF calculations indicate that the most stable conformers are *tttt1* and *tttt3*, which may suggest a geometric effect of the 180° dihedral angle allowing less strong repulsive forces between dendrimer atoms. However, when electron correlation is taken into account, the most stable conformers are those where the dihedral angle is close to 64° as observed in the ethylenediamine *gauche* conformer. Moreover, even when the *tttt2* conformer has a stabilizing hydrogen bond and *tttt3* has none, the energy difference between them is relatively small (0.65 kcal/mol for G0-NH_2 and 0.18 kcal/mol for G0-OH), with *tttt2* the most stable, suggesting that not only hydrogen bond interactions but also the magnitude of the core dihedral angle may contribute to the conformer stability.

Next we compare the geometrical and electronic properties (bond lengths, atomic charge distribution) predicted for individual isolated branches to those of G0. These comparisons permit us to assess the accuracy of a building procedure for higher generation dendrimers based on addition of such branches of known properties, using classical molecular mechanics and molecular dynamics, where the ab initio data presented in this paper are used to generate accurate effective force field models needed for a full atomic description as the dendrimer generation increases. Figure 2 shows three optimized structures for fragments: a 30-atom structure, designated as fragment 1 (F1), including the core molecule, EDA, with one of its amine hydrogen atoms substituted by an $-NH_2$-terminated branch, a second fragment of 44 atoms (F2) which reflects some characteristics from the core and surrounding atoms, and a third fragment of 29 atoms equivalent to F1 but with a −OH-terminated branch. The analogies and differences of the geometrical and electronic properties found for fragments F1, F2, and F3 optimized at the HF/3-21G and HF/6-31G(d) levels in comparison to those of the complete dendrimers are discussed in the next sections.

Atomic Charge Distribution. Given the somehow radial symmetry observed from our calculations, we organized and classified the G0-NH_2 and G0-OH atoms in types; the adopted nomenclature is listed in Table 2. Comparison of the charges in Table 3 for the full G0 conformers with those of the calculated fragments (Figure 2) indicates that the fragments describe very well the atomic Mulliken population charges, which suggests that such information could be used for effective force field parametrization of higher order dendrimers. Table 3 lists only the innermost atom charges of F2 and the outermost atoms of F1 and F3, since those atoms are the ones that best resemble the G0-NH_2 and G0-OH environments. Comparing the atomic charges among conformers, we observe that, in most cases, *tttt2* (the extended and more symmetric structure) shows the largest differences from the other two conformers.

Table 3 reveals the existence of three regions in the dendrimer structure—suitable for ion complexation or metal adsorption—where the distribution of the electron density generates an appropriate environment to attract either a positive ion or a neutral atom: the region next to CC, NC, CN3, and CCO, which is designated as the core site, the region next to the amide oxygen (O) and nitrogen (N2) atoms, called the amide site, and the region involving the terminal group N1 and surrounding atoms (CN1, CN2), called the amine site. Each of these sites has at least one strong electronegative atom inserted in a micropolarized environment including positive atoms such as H and the carbonyl carbon (CO). Table 3 also illustrates differences in Mulliken population charges due to the different terminal groups of PAMAM-G0. It is noticeable that the atomic charge varies significantly in the neighborhood of the terminal group whether it is $-NH_2$ or −OH. This suggests the possibility of selective behavior toward specific substrates and/or ligands, arising from the interactions of these terminal groups with the given surfaces/ligands. For example, the existence of negative charges on the primary amine terminal groups higher than those in the O atoms belonging to hydroxyl terminal groups in G0-OH, and also higher than the charges on the tertiary amines inside the dendrimer (atom type NC), explains the ease of the protonation found in primary amines with respect to that in tertiary amines.[19,41−44] Such charge distribution in PAMAM-

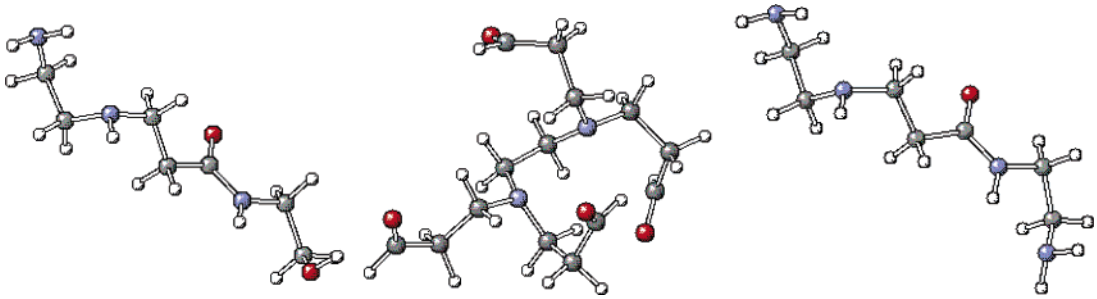

Figure 2. Optimized (HF/3-21G) fragment geometries: (a) 30-atom structure (F1), (b) 44-atom structure (F2), (c) 29-atom structure (F3).

TABLE 2: Nomenclature Used To Describe Atom Types in PAMAM-G0-NH_2 and -G0-OH

element	atom type	description
carbon	CC	C atom in the core
nitrogen	NC	N atom in the core
carbon	CN3	C atom in the branch bound to NC
carbon	CCO	C atom bound to CO
carbon	CO	C atom in the carbonyl group
nitrogen	N2	amide nitrogen
carbon	CN2	C atom bound to the amide nitrogen
carbon	CY	carbon atom bound to the terminal group atom
atom Y[a]	Y	terminal group atom
oxygen	O	oxygen in the carbonyl group
hydrogen	HCC	H atom bound to CC
hydrogen	HCN3	H atom bound to CN3
hydrogen	HCCO	H atom bound to CCO
hydrogen	HN2	H atom bound to N2
hydrogen	HCN2	H atom bound to CN2
hydrogen	HCY	H atom bound to CY
hydrogen	HY	H atom bound to Y

[a] Atom Y is designated to represent the terminal group atoms: N1 is the primary amine terminal nitrogen in G0-NH_2, and OT is the hydroxyl terminal oxygen in G0-OH.

TABLE 3: Mulliken Atomic Charges (B3LYP/6-31G(d)//HF/3-21G) Averaged over All Atoms of a Given Type (Nomenclature in Table 2) for G0-NH_2 and G0-OH[a]

	G0-NH_2				G0-OH			
atom type	*tttc*	*tttt1*	*tttt2*	F1 and F2	*tttc*	*tttt1*	*tttt2*	F2 and F3
CC	−0.17	−0.18	−0.15	−0.16	−0.16	−0.16	−0.15	−0.16
NC	−0.41	−0.40	−0.37	−0.39	−0.40	−0.40	−0.37	−0.39
CN3	−0.16	−0.16	−0.15	−0.16	−0.17	−0.16	−0.14	−0.16
CCO	−0.37	−0.37	−0.38	−0.39	−0.37	−0.37	−0.38	−0.38
CO	0.59	0.59	0.60	0.61	0.61	0.61	0.60	0.61
N2	−0.59	−0.59	−0.61	−0.60	−0.60	−0.60	−0.60	−0.60
CN2	−0.14	−0.14	−0.10	−0.11	−0.13	−0.13	−0.14	−0.12
CY	−0.13	−0.14	−0.16	−0.15	−0.06	−0.06	−0.05	−0.07
Y[b]	−0.74	−0.75	−0.76	−0.75	−0.65	−0.65	−0.63	−0.62
O	−0.53	−0.53	−0.54	−0.53	−0.54	−0.55	−0.53	−0.52
HCC	0.16	0.16	0.13	0.15	0.15	0.15	0.14	0.15
HCN3	0.15	0.15	0.16	0.16	0.16	0.16	0.16	0.16
HCCO	0.17	0.17	0.15	0.16	0.17	0.16	0.16	0.16
HN2	0.34	0.34	0.35	0.31	0.36	0.36	0.35	0.33
HCN2	0.15	0.15	0.16	0.16	0.16	0.16	0.17	0.16
HCY	0.15	0.15	0.14	0.14	0.15	0.15	0.15	0.15
HY	0.31	0.31	0.31	0.33	0.42	0.42	0.40	0.40

[a] Values in italics in the columns labeled "F1 and F2" correspond to fragment F2, and the nonitalic values in the same column correspond to fragments F1 and F3. [b] Atom Y is designated to represent the terminal group atoms: N1 is the primary amine terminal nitrogen in G0-NH_2, and OT is the hydroxyl terminal oxygen in G0-OH.

G0-NH_2 is a precursor of the picture observed in higher generation dendrimers;[44] a less polar environment is found in the interior with respect to that in the periphery.

Structural Analysis of G0 Conformers. Calculated values of bond lengths and angles were averaged among those of the same type; complete tables are available as Supporting Information. Engh and Huger[45] reported average bond lengths and bond angles for common amino acids and polypeptide backbones on the basis of a statistical survey of X-ray structures of small related chemical compounds taken from the Cambridge Structural Database. From the list of atom types defined in their study, we have established equivalences; for example, CCO in Table 2 is compared with their CH2G, which is the C_α for glycine. Thus, we are able to compare calculated bond lengths and angles concerning the peptide units present in the PAMAM-G0 branches with experimental data of similar compounds.

To simplify the nomenclature, we refer to the HF/3-21G optimizations as method I, to HF/6-31G(d) as method II, and to B3LYP/6-311G(d) as method III; the first two are applied to all the conformers (except *tttt3*), and method III is only applied to *tttt1*. For the carbonyl bond length in G0-NH_2 branches, method III gives a distance of 1.228 Å in close agreement with the reported average value 1.231 Å (standard deviation, std dev, 0.020 Å). Methods I and II yield 1.223−1228 and 1.204−1.208 Å for this bond length, respectively. For G0-OH we obtained 1.227−1.229, 1.207−1.208, and 1.227 Å using methods I, II, and III, respectively. Again, methods I and III provide a fairly good prediction, and method II yields a value that differs by at least 1 std dev from the averaged X-ray value.

Regarding the C−N amide bond, the average experimental value is 1.329 Å (std dev 0.014 Å) whereas for G0-NH_2 the predictions given by methods I, II, and III are 1.344−1.347, 1.346−1.348, and 1.357 Å, and for G0-OH, methods I, II, and III yield 1.344−1.347, 1.345−1.347, and 1.358 Å. In all cases, predictions are 1 std dev from the reported value for this bond, with HF yielding slightly better results than DFT.

The average experimental value for the N−C_α bond length is 1.451 Å (std dev 0.016 Å). For G0-NH_2, method III performed the best (1.454 Å) whereas methods I and II yield 1.455−1.467 and 1.445−1.448 Å, which are also in fair agreement with the expected value, and the same trend is found for G0-OH with calculated values of 1.457−1.459, 1.445−1.448, and 1.454 Å according to methods I, II, and III, respectively. The bond length reported for C−C_α is 1.516 Å (std dev 0.018 Å). For G0-NH_2, methods I, II, and III yield 1.518−1.520, 1.519−1.522, and 1.528 Å, respectively. For G0-OH, the respective calculated values are 1.516−1.517, 1.518−1.519, and 1.524 Å, also in close agreement with the experimental value. Thus, regardless of the method used, calculated bond lengths except those for the carbonyl bond at HF/6-31G(d) are in fair agreement with values measured for proteins that contain the same secondary amide group characteristic of the PAMAM branches.

The experimental value for the angle C_α−C−O is 120.8° (std dev 2.1°). Predictions for the equivalent angle type CCO−CO−O are 119.4−122.1°, 121.3−122.3°, and 121.4° for G0-NH_2 and 121.7−122.3°, 120.8−121.2°, and 121.8° for G0-OH according to methods I, II, and III, respectively, in close

agreement (within 1 std dev) with experiment. A value of 123° (std dev 1.6°) is reported for the O−C−N angle (O−CO−N2 according to Table 2). Methods I, II, and III yield 122.2−122.9°, 122.0−122.8°, and 122.9° for G0NH$_2$ and 122.0−122.6°, 122.0−122.8°, and 122.5° for G0-OH, respectively, again in close agreement with experiment. Very good agreement is also found for the C_α'−C−N (CCO−CO−N2) angle calculated as 115.0−117.7°, 115.3−116.5°, and 115.7° for G0-NH$_2$ according to methods I, II, and III, respectively, and 115.4−116.3°, 116.0−117.1°, and 115.7° for G0-OH, whereas the experimental value is 116.4° (std dev 2.1°). For the angle C−N−C_α (CN2−N2−CO in our nomenclature) methods I, II, and III yield 121.0−122.6°, 121.3−123.2°, and 123.0° for G0-NH$_2$ and 122.2−124.0°, 122.6−124.4°, and 123.1° for G0-OH, whereas the averaged X-ray values yield 120.6° (std dev 1.7°). On the other hand, the predicted values for the angle C−N−H (CO−N2−HN2) with methods I, II, and III are 119.9−122.9°, 118.5−122.3°, and 120.1° for G0-NH$_2$, whereas for G0-OH they are 120.1−121.9°, 117.9−119.7°, and 119.6°, respectively, which compare very well with the experimental value of 119.5°.[46] Finally, for the angle H−N−C_α (CN2−N2−HN2) methods I, II, and III yield 114.7−119.0°, 115.7−118.5°, and 114.5° for G0-NH$_2$ and 115.8−116.1°, 116.8−117.0°, and 116.6° for G0-OH, respectively, whereas the experimental value is 118.2°.[46]

Additionally, when angles around the carbonyl carbon (atom type CO) and the amide nitrogen (atom type N2) are summed, we obtain values close to 360° regardless of the method and of the dendrimer, which is not surprising because the carbonyl carbon and the secondary amide nitrogen are planar centers with no tendency for pyramidalization of the nitrogen atom as is known to occur in tertiary amines in which the nitrogen lone pair is not delocalized as it is in the amide bond where resonance effects take place. Moreover, the calculated values of the dihedral ω (C_α−C−N−C_α') are close to 180°, thus implying planarity, except for the value corresponding to one branch of G0-NH$_2$ that reached 160° for *tttt1* at HF/6-31G(d), HF/6-311G-(d), and B3LYP/6-311G(d). The value of ω is close to 0° (4.9° at HF/3-21G and 6.1° at HF/6-31G(d)) for the branch that has its secondary amide group in the *cis* position in the conformer *tttc*.

To characterize the core, we compare the calculated values with those available for EDA:[47] a C−N bond length of 1.469 Å, a C−C bond length of 1.545 Å, a C−H bond length of 1.11 Å, and a dihedral angle formed by the planes NCC and CCN equal to 64° corresponding to a lower energy *gauche* conformer. Calculations with methods I, II, and III for the C−C bond length (bond type CC−CC) yield 1.534−1.542, 1.529−1.534, and 1.533 Å for G0-NH$_2$ and 1.536−1.543, 1.529−1.534, and 1.531 Å for G0-OH, respectively. For G0-NH$_2$, the same methods yield 1.457−1.472, 1.446−1.456, and 1.466 Å for the C−N bond length, and for G0-OH, the methods yield 1.459−1.472, 1.446−1.456, and 1.467 Å for the C−N bond length. Methods I, II, and III for the dihedral angle N−C−C−N yield values that span 42.7−57.6°, 55.2−57.5°—with the lowest value corresponding to that from the fragment F2 and the highest to that from *tttt2*—and 49° for G0-NH$_2$, whereas the same methods yield 51.5−58°, 53.7−58°, and 54.2° for G0-OH. As mentioned in the previous section, the stable G0 *tttt3* conformer, having intra-branch N−H···N−H$_2$ interactions in its four branches, has a value of 180° for this dihedral angle. We speculate that during the ion (metal atom) complexation process, such a dihedral angle could be reduced, creating a favorable environment for the complexation process in core and amide sites. Geometric and electronic effects will determine whether a given ion/atom guest is accepted inside the dendrimer next to the core region. An opening of the NCCN core dihedral angle up to 180° may weaken the interbranch H-bonds, allowing larger guests to be hosted. On the other hand, a closure of the dihedral angle down to 64° or less would allow better interbranch H-bond interactions, admitting smaller guests. Some of these aspects are tested with calculations of naked and solvated ion (metal atom) complexation.[48]

It is noticeable that a significant opening of the angle formed by the primary amines with H atoms (angle type HN1−N1−HN1) in each terminus of EDA takes place when branches are added to that terminal group (angle type CN3−NC−CN3). Methods I, II, and III predict an angle change from 110.8−112.4° to about 115.6−119.1°, from 107.0−112.4° to 114.8−119.1°, and from 106.8° to 113.4°, respectively. It is also observed after simulations performed on EDA molecules that the inward orientation of the terminal groups—which stabilize the *gauche* conformer through hydrogen bonding—changes to an outward orientation. This is not surprising because the presence of branches promotes mutual repulsion among the branches, especially those starting at the same N atom. This pattern is expected to be repeated as the dendrimer generation grows.

In summary, calculated bond lengths, angles, and dihedral angles are in agreement with the values expected for the corresponding bond and angle types,[45] and small variations are detected as the basis sets are augmented for the HF-optimized geometries as reported by Hehre et al.[49] The comparisons presented in this section, along with the results from Table 1, validate the methodology used to determine the structure and identification of lowest energy conformers of these macromolecular systems.

IR Vibrational Spectra. We report calculations for the *tttc*, *tttt1*, *tttt2*, and *tttt3* conformers of G0-NH$_2$ (Table 4) and G0-OH (Table 5) at HF/6-31G(d), and those for the most stable conformer (*tttt1*) at HF/6-311G(d) and B3LYP/6-311G(d) of both dendrimers (Table 6). Assignments of calculated vibrational frequencies and IR intensities are done on the basis of agreement with published experimental IR data of compounds containing similar functional groups[50,51] and by visual analysis of the calculated normal mode displacement vectors. Frequencies are usually assigned to individual motions,[52] because it is useful to identify the major cause of any band. However, absorption bands of molecules cannot strictly be considered due to a single vibration source, since the whole molecule is involved.[50] This is especially noticed in compounds containing amides as functional groups. Amide bands include the amide A band, which is primarily a N−H stretch mode, the amide I band, a C═O stretch with a minor contribution from the in-plane C−N−H angle bending, the amide II involving an out-of-phase combination of largely N−H in-plane bending and a C−N stretch, the amide III including an in-phase combination of N−H in-plane bending and a C−N stretch, the amide IV resulting from an in-plane C═O deformation mode, the amide V, a N−H out-of-plane deformation, the amide VI, a C═O out-of-plane deformation, and the amide VII mode involving out-of-plane CN torsions.[53,54]

Intensities shown in Tables 4−6 correspond to maxima in the peaks obtained after the frequencies were scaled and a 50/50 combination of Lorentzian and Gaussian functions was applied at intervals of 2 cm^{-1} with a bandwidth at half-height of 20 cm^{-1}. Although vibrational frequencies could be interpreted with great accuracy, vibrational intensities are particularly difficult to predict through ab initio methods,[55] because they

TABLE 4: Calculated G0-NH_2 IR Frequencies (cm^{-1}) (HF/6-31G(d), Scaling Factor of 0.8953[56,57]) and Assignments[a]

tttc		*tttt1*		*tttt2*		*tttt3*		
freq	intens	freq	intens	freq	intens	freq	intens	assignment
288	0.076	288	0.123	282	0.206	282	0.119	amide VII + NH_2 torsion
496	0.057	490	0.071	500	0.063			CCN tors
564	0.207	572	0.317	540	0.317	546	0.458	amide V + IV
604	0.201	614	0.334	622	0.119	636	0.085	amide V + VI
714	0.108	724	0.037	752	0.030	730	0.058	amide VI + CH_2 rocking
822	0.160	816	0.125	810	0.235	810	0.313	NH_2 wag
918	0.311	920	0.343	898	0.486	900	0.532	CCN sym stretch + NH_2 wag + CH_2 rocking
986	0.105	980	0.138	984	0.174	986	0.095	CH_2 rocking + CC stretch
1028	0.123	1032	0.095	1028	0.153	1024	0.212	CH_2 rocking
				1054	0.136	1050	0.164	CH_2 rocking + CCN asym stretch
1068	0.091	1066	0.087	1064	0.142	1066	0.150	CCN asym stretch
1098	0.057	1096	0.087	1094	0.119	1098	0.153	CH_2 twist + CCN asym stretch
1134	0.092	1128	0.074	1134	0.173	1124	0.153	CH_2 twist
1166	0.138	1172	0.124	1172	0.125	1168	0.115	CH_2 twist + NH_2 twist
1202	0.088	1208	0.099	1226	0.292	1212	0.272	amide III
1262	0.267	1266	0.413	1262	0.461	1260	0.449	amide III + CH_2 twist + NH_2 twist
1324	0.196	1322	0.120	1314	0.294	1320	0.148	CH_2 twist + NH_2 twist + CH_2 wag
1384	0.221	1390	0.181	1392	0.352	1408	0.302	CH_2 wag
1492	0.283	1462	0.089	1490	0.241	1490	0.224	CH_2 scissors
1534	0.811	1534	1.578	1530	2.140	1528	2.888	amide II
1646	0.140	1656	0.222	1646	0.302	1644	0.255	NH_2 scissors
1718	1.499	1716	1.330	1734	1.261	1732	1.535	amide I
2840	0.345	2842	0.402	2842	0.507	2834	0.605	CH_2 sym stretch
2856	0.382	2858	0.333			2850	0.610	CH_2 sym stretch
2896	0.307	2900	0.446	2908	0.483	2916	0.425	CH_2 asym stretch + sym stretch
2918	0.234							CH_2 asym stretch + sym stretch
2948	0.205	2952	0.259	2964	0.242	2956	0.281	CH_2 asym stretch
3334	0.101	3338	0.126	3338	0.012	3340	0.008	NH_2 sym stretch
3424	0.278	3424	0.432	3432	0.444	3418	0.017	NH_2 asym stretch
3470	0.113	3472	0.176	3474	0.306	3474	0.305	amide A

[a] Reported intensities are the result of smoothing over calculated values (see the text). Corresponding spectra are not shown.

TABLE 5: Calculated G0-OH IR Frequencies (cm^{-1}) (HF/6-31G(d), Scaling Factor of 0.8953) and Assignments[a]

tttc		*tttt1*		*tttt2*		*tttt3*		
freq	intens	freq	intens	freq	intens	freq	intens	assignment
322	0.400	322	0.567	326	0.577	324	0.541	OH tors
530	0.281	538	0.583	514	0.484	512	0.439	CCN tors + amide V
600	0.501	600	0.757	648	0.132			amide V + OH out-of-plane bending
712	0.105	720	0.060	724	0.026	722	0.052	amide VI + amide V
830	0.031	822	0.062	830	0.039	834	0.038	amide V
976	0.072	986	0.115	980	0.189	990	0.057	CCC stretch + CH_2 rocking
1026	0.183	1026	0.259	1024	0.335	1026	0.295	CH_2 rocking + OH in-plane bending
1090	0.328	1090	0.568	1088	0.547	1088	0.432	CCO stretch
1220	0.113	1222	0.165	1226	0.483	1210	0.469	amide III + CH_2 twist + OH in-plane bending
1252	0.282	1250	0.445	1250	0.562	1250	0.407	amide III
1328	0.224	1326	0.140	1314	0.432	1334	0.139	CH_2 wag +CH_2 twist
1410	0.338	1408	0.480	1394	0.513	1406	0.383	CH_2 wag + OH in-plane bending
1492	0.256			1480	0.202	1486	0.14	CH_2 scissors
1540	0.792	1530	1.878	1532	2.100	1530	2.08	amide II
1714	1.282	1716	1.458	1734	1.530	1738	1.36	amide I
2860	0.322	2860	0.545	2850	0.431	2846	0.349	CH_2 sym stretch
2878	0.381	2878	0.664	2876	0.541	2876	0.461	CH_2 sym stretch
2924	0.344	2922	0.547	2902	0.688	2896	0.36	CH_2 sym stretch + asym stretch
		2948	0.426	2950	0.335	2952	0.328	CH_2 asym stretch
3438	0.242	3434	0.276	3438	0.483			amide A
				3482	0.308	3478	0.207	amide A
3594	0.894	3596	1.401					amide A + OH stretch
3672	0.130	3672	0.222	3674	0.209	3672	0.193	OH stretch

[a] Reported intensities are the result of smoothing over calculated values (see the text).

are determined mainly by fluctuations of atomic electric charges accompanying particular vibrational modes and their associated spatial motion given by vibrational eigenvectors. Thus, we do not claim that we have found the true intensities corresponding to every mode reported.

The assigned frequencies listed in Tables 4−6 correspond to positions of the peaks in the smoothed spectra (where the calculated and scaled ab initio harmonic frequencies are the red lines shown in Figure 3). It is observed that the intensities are sometimes affected by smoothing, such as the ratio of the relative intensities of amide I and amide II bands, which was reverted for G0-OH when smoothing was applied (Figure 3b). The assignment was completed by comparing our findings with the values reported in the literature for dendrimers and similar molecules containing secondary amide groups. Scaling factors of 0.8953 and 0.9047 were applied to the calculated frequencies

TABLE 6: Calculated IR Frequencies (cm^{-1}) for *tttt1* Conformers of G0-NH_2 and G0-OH at HF/6-311G(d) and B3LYP/6-311G(d)[a]

G0-NH_2					G0-OH				
HF		DFT			HF		DFT		
freq	intens	freq	intens	assignment	freq	intens	freq	intens	assignment
290	0.135	250	0.109	amide VII + NH_2 rocking	318	0.577	348	0.571	OH tors
494	0.075	516	0.066	CCN tors	490	0.189	518	0.104	CCN tors
578	0.396	596	0.109	amide V + amide IV	546	0.548	558	0.158	amide V
618	0.390	620	0.138	amide V + amide VI	608	0.629	592	0.372	amide V + amide IV
688	0.030	670	0.424	amide V	698	0.029	694	0.932	OH out-of-plane bending + amide V
732	0.038	754	0.084	amide VI + CH_2 rocking	728	0.054	748	0.073	amide VI + amide V
822	0.132	824	0.147	NH_2 wag	828	0.061	836	0.044	amide V
886	0.219	894	0.358	CCN sym stretch + NH_2 wag + CH_2 rocking	862	0.055	866	0.047	CCC sym stretch + CCO sym stretch
924	0.381	936	0.435	NH_2 wag + CH_2 rocking	900	0.067	916	0.071	CH_2 rocking + amide VI + CCO sym stretch
988	0.155	966	0.296	CH_2 rocking + CC stretch	992	0.109	994	0.180	CCC asym stretch + CH_2 rocking
1012	0.153	1018	0.127	CH_2 rocking	1034	0.238	1050	0.266	CH_2 rocking + OH in-plane bending
1038	0.118			CH_2 rocking + CCN asym stretch	1096	0.544	1080	0.495	CCO asym stretch
1072	0.111	1086	0.130	CCN asym stretch	1128	0.206	1140	0.185	CN stretch + CO stretch
1104	0.105	1114	0.159	CH_2 twist + CCN asym stretch	1174	0.232	1178	0.117	CH_2 twist
1136	0.082	1144	0.117	CH_2 twist	1192	0.235			CH_2 twist + OH in-plane bending
1184	0.160	1206	0.142	CH_2 twist + NH_2 twist	1228	0.209	1212	0.207	amide III + CH_2 twist + OH in-plane bending
1216	0.139	1230	0.133	amide III	1262	0.503	1270	0.547	amide III
1272	0.516	1278	0.493	amide III + CH_2 twist + NH_2 twist			1302	0.366	amide III + CH_2 twist
1330	0.159	1334	0.152	CH_2 twist + NH_2 twist + CH_2 wag	1336	0.154	1344	0.183	CH_2 wag + CH_2 twist
1398	0.202	1388	0.247	NH_2 twist + CH_2 wag	1384	0.296			CH_2 wag + CH_2 twist
		1418	0.117	CH_2 wag	1406	0.435	1394	0.344	CH_2 wag + OH in-plane bending
1468	0.113			CH_2 scissors	1422	0.456	1416	0.295	OH in-plane bending + CH_2 wag + CH_2 scissors
1548	1.886	1544	1.960	amide II			1438	0.320	CH_2 scissors + OH in-plane bending + CH_2 wag
1716	1.529	1704	1.570	amide I	1492	0.202			CH_2 scissors
2822	0.242			CH_2 sym stretch	1546	1.918	1550	1.709	amide II
2852	0.521	2830	0.284	CH_2 sym stretch	1718	1.412	1702	1.674	amide I
2908	0.621	2888	0.620	CH_2 sym stretch + CH_2 asym stretch	2816	0.220	2818	0.188	CH_2 sym stretch
2966	0.353	2948	0.515	CH_2 asym stretch	2838	0.241	2832	0.211	CH_2 sym stretch
		3346	0.403	NH_2 sym stretch	2868	0.591	2860	0.257	CH_2 sym stretch
3392	0.121	3374	0.766	NH_2 sym stretch	2892	0.703	2892	0.514	CH_2 sym stretch
		3424	0.241	NH_2 asym stretch	2936	0.603	2922	0.664	CH_2 sym stretch + CH_2 asym stretch
3482	0.358	3470	0.206	amide A	2962	0.485	2970	0.544	CH_2 asym stretch
					3488	0.239	3494	2.032	amide A
					3692	1.116	3646	0.079	OH stretch

[a] A scaling factor of 0.9047[57] was used for the HF calculations, and the dual scaling scheme[58] (see the text) was employed for the DFT frequencies. Reported intensities are the result of smoothing (blue curves, Figure 3) over calculated values (red lines, Figure 3).

at HF/6-31G(d) and HF/6-311G(d), respectively.[56,57] A dual scaling scheme with a factor of 0.9659 to scale frequencies lower than 1800 cm^{-1} and 0.9927 for frequencies higher than 1800 cm^{-1} was employed for the B3LYP frequencies as recommended by Halls et al.[58]

The calculated HF/6-31G(d) intensity of the amide I band (Tables 4 and 5) is higher than that of the amide II band not only for G0-NH_2 (*tttc*) but also for G0-OH (*tttc*), in agreement with experiment,[31,53,54] but the trend reverts for the G0-NH_2 *tttt1*, *tttt2*, and *tttt3* conformers. Such disagreement between theory and experiment, which may be attributed to solvent effects not present in the calculated spectra, has been observed also in other calculated spectra for chemical compounds containing secondary amide groups such as oligopeptides.[59]

For *tttt1*, compared to experimental values of amide-containing compounds,[31,60] the HF/6-311G(d) and B3LYP/6-311G(d) calculated amide I mode appears at a higher frequency (1716/1704 cm^{-1} for G0-NH_2 and 1718/1702 cm^{-1} for G0-OH, Table 6); this difference may originate in the effect of intermolecular hydrogen bonds[53] that lower this frequency in solution compared to the gas-phase data calculated here. The frequencies corresponding to the amide II band (1548/1544 cm^{-1} for G0-NH_2 and 1546/1550 cm^{-1} for G0-OH) are in better agreement with reported experimental values.[31,60]

The amide III band (1272/1278 cm^{-1} for G0-NH_2 and 1262/1270 cm^{-1} for G0-OH, Table 5) is a medium-intensity mode that also is noticeable in the spectra for the conformers calculated at HF/6-31G(d) (Tables 4 and 5); the calculated frequencies are lower than those reported for G4-NH_2 (1358 cm^{-1}),[31] but in close agreement with those calculated for solid *N*-methylformamide by Bour et al. [59] For G0-NH_2 this mode is mixed with the CH_2 and NH_2 twisting modes. So, another peak is detected at 1216/1230 cm^{-1} for this amide III mode. As it is not easy to assign peaks in regions where intensive coupling of modes exists, the peak assignments in these regions refer to the most important mode but not necessarily the only one present.

Similarly, the fingerprint region of the spectra (amides IV, V, and VI) is the most interesting but also hardest to analyze because of coupling of the various modes. Regarding the amide V mode, it may not be distinguished from strong CH_2 rocking modes and OH in-plane bending for G0-NH_2 and G0-OH respectively, and is strongly sensitive to the molecular geometry especially due to a H-bonding effect that shifts it to higher frequencies.[54] The amide VI mode, which is coupled to the CH_2

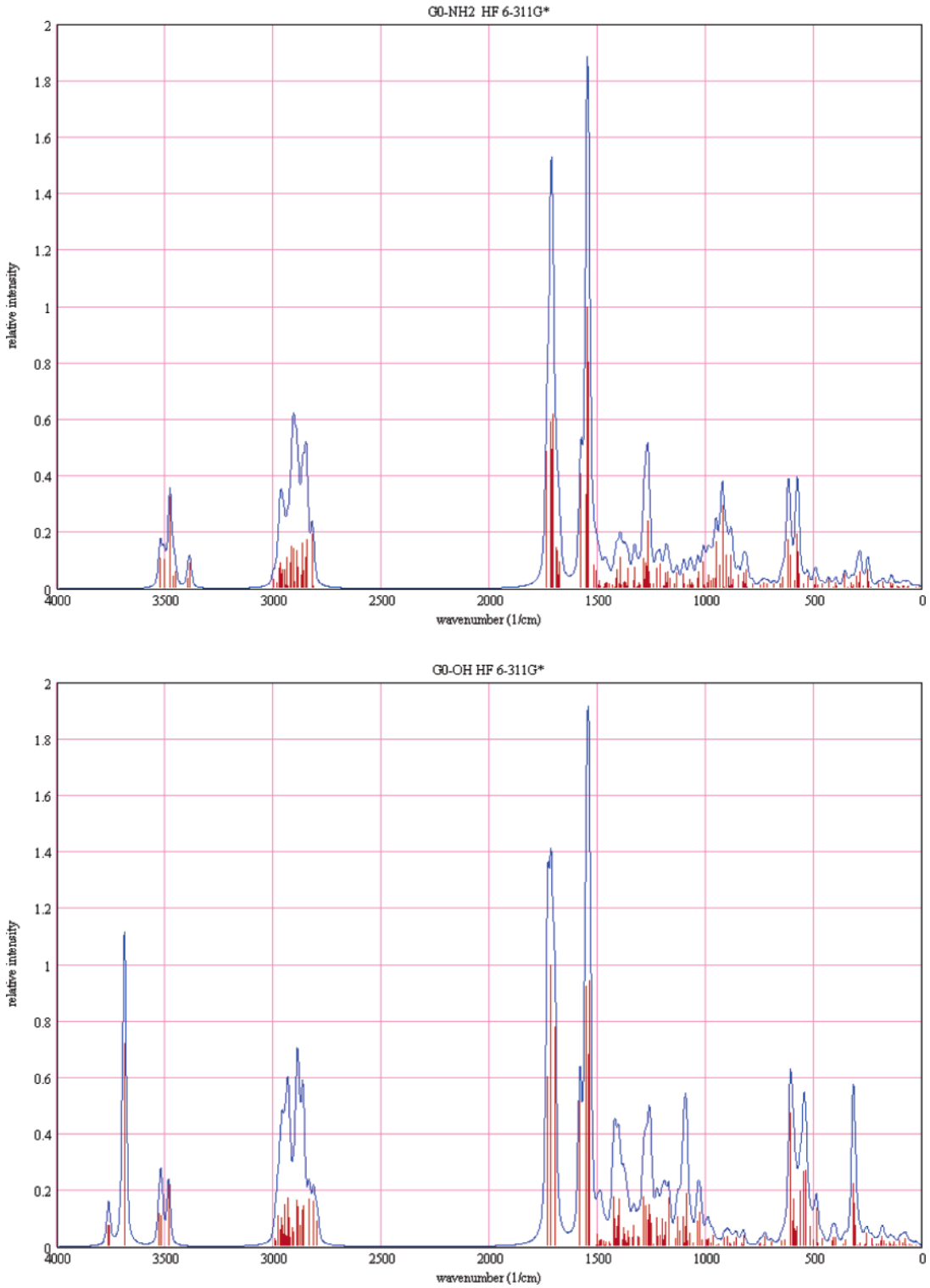

Figure 3. Calculated (HF/6-311G(d)) IR vibrational spectra for G0-NH_2 (top) and G0-OH (bottom). The red lines are the calculated intensities normalized with respect to the maximum value of each spectrum. The blue curves are the result of smoothing using a 50/50 combination of Lorentzian and Gaussian functions at intervals of 2 cm^{-1} with a bandwidth at half-height of 20 cm^{-1}.

rocking modes, appears at 732/754 cm^{-1} for G0-NH_2 and is coupled to the amide V mode at 728/748 cm^{-1} for G0-OH (Table 6). This mode is of medium to weak intensity and is also affected by H-bonding that shifts it to higher frequencies,[54] whereas the amide IV mode is only weakly affected by H-bonding.[54] The calculated amide mode A, mainly composed of NH stretching, is observed at 3482/3470 cm^{-1} for G0-NH_2, whereas for G0-OH it is observed at 3488/3494 cm^{-1} (Table 6), which may be compared with the value of 3272 cm^{-1} reported for G4-NH_2.[31] For G0-OH we could not distinguish clearly the amide VII modes, but they are assigned for G0-NH_2 even though they are mixed with NH_2 torsion modes at 290/250 cm^{-1}, which according to the work of Papanek et al.[54] is expected in the region 200−300 cm^{-1}.

Regarding the other modes assigned in Table 6, it is worth highlighting the CCN asymmetric stretching at 1072/1080 cm^{-1} and the CCN symmetric stretching at 886/894 cm^{-1} values in agreement with results reported for alanine by Diem et al.[61]

For G0-OH, the CCO asymmetric stretching is a medium-intensity mode noticeable at 1096/1080 cm^{-1} along with the CCO symmetric stretching mixed with CCC stretching at 862/866 cm^{-1}.

Conclusions

Analysis of the HF and DFT fully optimized structures of PAMAM-G0-NH_2 and -G0-OH indicate that *tttt* conformers (all branches in the *trans* position), in highly intramolecularly interactive conformations, are the most stable in the gas phase, where an important role is played by intramolecular hydrogen bonds and other interbranch interactions in the stabilization of PAMAM-G0 dendrimers.

Three regions of the dendrimer structure are found suitable for ion complexation or metal adsorption, where the distribution of the electron density generates an appropriate environment to attract either a positive ion or a neutral atom: one next to the core site, another including the amide oxygen and nitrogen atoms, and a third involving the terminal group and surrounding atoms. Each of these sites has at least one strong electronegative atom inserted in a micropolarized environment including positive atoms such as H and the carbonyl carbon atoms.

A strong variation of the atomic charge is found in the neighborhood of the terminal group whether it is $-NH_2$ or $-OH$, suggesting the possibility of selective behavior toward specific substrates and/or ligands, arising from the interactions of these terminal groups with the given surfaces/ligands. The charge distribution in PAMAM-NH_2 also indicates that the terminal primary amines are more basic than the tertiary (core) amines. This result explains the experimentally found ease of protonation of primary compared to tertiary amines. Such charge distribution in PAMAM-G0-NH_2 is a precursor of the less polar environment found in the interior of higher generation dendrimers, with respect to that in the periphery.

Vibrational spectra for G0-NH_2 and G0-OH are fully described; the main features agree with trends expected for compounds containing a secondary amide group. Also the geometric parameters (bond lengths and angles) around this peptide bond are in fair agreement with those expected in proteins.

Acknowledgment. This work is supported by National Science Foundation Grant CTS-0103135. Supercomputer resources granted by the National Energy Research Scientific Computing Center (NERSC), by the DoD Major Shared Resource Centers (ARL MSRC and ASC MSRC), and by the National Center for Supercomputer Applications under Grant CTS030036 are gratefully acknowledged.

Supporting Information Available: Average bond lengths and angles for conformers G0-NH_2 and G0-OH. This material is available free of charge via the Internet at http://pubs.acs.org.

References and Notes

(1) Frechet, J. M. J. *J. Polym. Sci., Part A: Polym. Chem.* **2003**, *41*, 3713.
(2) Esumi, K. *Top. Curr. Chem.* **2003**, *227*, 31.
(3) Newkome, G. R.; Moorefield, C. N.; Vogtle, F. *Dendrimers and Dendrons: Concepts, Syntheses, Applications*; Wiley-VCH: Weinheim, Germany, 2001.
(4) *Dendrimers and other dendritic polymers*; Frechet, J. M. J., Tomalia, D. A., Eds.; John Wiley & Sons: New York, 2002.
(5) Balogh, L.; Tomalia, D. A.; Hagnauer, G. L. *Chem. Innovation* **2000**, *30*, 19.
(6) Crooks, R. M.; Lemon, B. I., III; Sun, L.; Yeung, L. K.; Zhao, M. *Top. Curr. Chem.* **2001**, *212*, 81.
(7) Balogh, L.; Tomalia, D. *J. Am. Chem. Soc.* **1998**, *120*, 7355.
(8) Sooklal, K.; Hanus, L. H.; Ploehn, H. J.; Murphy, C. J. *Adv. Mater.* **1998**, *10*, 1083.
(9) Tomalia, D. A.; Naylor, A. M.; Goddard, W. A. *Angew. Chem., Int. Ed. Engl.* **1990**, *29*, 138.
(10) Zhao, M.; Sun, L.; Crooks, R. M. *J. Am. Chem. Soc.* **1998**, *120*, 4877.
(11) Zhao, M.; Crooks, R. M. *Adv. Mater.* **1999**, *11*, 217.
(12) Zhao, M.; Crooks, R. M. *Chem. Mater.* **1999**, *11*, 3379.
(13) Zhao, M.; Crooks, R. M. *Angew. Chem., Int. Ed.* **1999**, *38*, 364.
(14) Esumi, K.; Susuki, A.; Yamahira, A.; Torigoe, K. *Langmuir* **2000**, *16*, 2604.
(15) Barron, J. A.; Bernhard, S.; Houston, P. L.; Abruna, H. D. *J. Phys. Chem. A* **2003**, *107*, 8130.
(16) Bao, C.; Jin, M.; Lu, R.; Zhang, T.; Zhao, Y. Y. *Mater. Chem. Phys.* **2003**, *81*, 160.
(17) Furer, V. L.; Kovalenko, V. I.; Vandyukov, A. E.; Majoral, J. P.; Caminade, A. M. *Spectrochim. Acta* **2002**, *58*, 2905.
(18) Kovalenko, V. I.; Furer, V. L.; Vandyukov, A. E.; Shagidullin, R. R.; Majoral, J. P.; Caminade, A. M. *J. Mol. Struct.* **2002**, *604*, 45.
(19) Cakara, D.; Kleimann, J.; Borkovec, M. *Macromolecules* **2003**, *36*, 4201.
(20) Zhou, L.; Russell, D. H.; Zhao, M.; Crooks, R. M. *Macromolecules* **2001**, *34*, 3567.
(21) Ottaviani, M. F.; Montalti, F.; Turro, N. J.; Tomalia, D. A. *J. Phys. Chem. B* **1997**, *101*, 158.
(22) Ottaviani, M. F.; Valluzzi, R.; Balogh, L. *Macromolecules* **2002**, *35*, 5105.
(23) Pellechia, P. J.; Gao, J.; Gu, Y. L.; Ploehn, H. J.; Murphy, C. J. *Inorg. Chem.*, *43*, 1421.
(24) Canetta, E.; Maino, G. *Nucl. Instrum. Methods Phys. Res., B* **2004**, *213*, 71.
(25) Cagin, T.; Wang, G.; Martin, R.; Breen, N.; Goddard, W. A. *Nanotechnology* **2000**, *11*, 77.
(26) Karatasos, K.; Adolf, D. B.; Davies, G. R. *J. Chem. Phys.* **2001**, *115*, 5310.
(27) Naylor, A. M.; Goddard, W. A.; Kiefer, G. E.; Tomalia, D. A. *J. Am. Chem. Soc.* **1989**, *111*, 2339.
(28) Cagin, T.; Wang, G.; Martin, R.; Zamanakos, G.; Vaidehi, N.; Mainz, D. T.; Goddard, W. A. *Comput. Theor. Polym. Sci.* **2001**, *11*, 345.
(29) Gotze, I. O.; Likos, C. N. *Macromolecules* **2003**, *36*, 8189.
(30) Lin, C.; Wu, K.; Sa, R.; Mang, C.; Liu, P.; Zhuang, B. *Chem. Phys. Lett.* **2002**, *363*, 343.
(31) Manna, A.; Imae, T.; Aoi, K.; Okada, M.; Yogo, T. *Chem. Mater.* **2001**, *13*, 1674.
(32) Davis, A. P.; Ma, G.; Allen, H. C. *Anal. Chim. Acta* **2002**, *224141*, 1.
(33) Petty, R.; Altomare, D.; Balbuena, P. B. AIChE National Meeting, Indianapolis, IN, 2002.
(34) Halls, M. D.; Tripp, C. P.; Schlegel, H. B. *Phys. Chem. Chem. Phys.* **2001**, *3*, 2131.
(35) Friesner, R. A.; Dunietz, B. D. *Acc. Chem. Res.* **2001**, *34*, 351.
(36) Mulliken, R. S. *J. Chem. Phys.* **1955**, *23*, 1833.
(37) Mulliken, R. S. *J. Chem. Phys.* **1955**, *23*, 1841.
(38) Mulliken, R. S. *J. Chem. Phys.* **1955**, *23*, 2338.
(39) Frisch, M. J.; Trucks, G. W.; Schlegel, H. B.; Scuseria, G. E.; Robb, M. A.; Cheeseman, J. R.; Zakrzewski, V. G.; Montgomery, J. A.; Stratmann, R. E.; Burant, J. C.; Dapprich, S.; Millam, J. M.; Daniels, A. D.; Kudin, K. N.; Strain, O. F. M. C.; Tomasi, J.; Barone, B.; Cossi, M.; Cammi, R.; Mennucci, B.; Pomelli, C.; Adamo, C.; Clifford, S.; Ochterski, J.; Petersson, G. A.; Ayala, P. Y.; Cui, Q.; Morokuma, K.; Malick, D. K.; Rabuck, A. D.; Raghavachari, K.; Foresman, J. B.; Ciolovski, J.; Ortiz, J. V.; Stefanov, V. V.; Liu, G.; Liashensko, A.; Piskorz, P.; Komaroni, I.; Gomperts, R.; Martin, R. L.; Fox, D. J.; Keith, T.; Al-Laham, M. A.; Peng, C. Y.; Nanayakkara, A.; Gonzalez, C.; Challacombe, M.; Gill, P. M. W.; Johnson, B.; Chen, W.; Wong, M. W.; Andres, J. L.; Head-Gordon, M.; Replogle, E. S.; Pople, J. A. *Gaussian 98*, revision A.11; Gaussian Inc.: Pittsburgh, PA, 1998.
(40) Jorgensen, W. L.; Gao, J. *J. Am. Chem. Soc.* **1988**, *110*, 4212.
(41) Tomalia, D. A.; Baker, H.; Dewall, J.; Hall, M.; Kallos, G.; Martin, S.; Roeck, J.; Ryder, J.; Smith, P. *Polym. J.* **1985**, *17*, 117.
(42) Diallo, M. S.; Balogh, L.; Shafagati, A.; Johnson, J. H.; Goddard, W. A.; Tomalia, D. A. *Environ. Sci. Technol.* **1999**, *33*, 820.
(43) Crooks, R. M.; Zhao, M.; Sun, L.; Chechik, V.; Yeung, L. K. *Acc. Chem. Res.* **2001**, *34*, 181.
(44) Niu, Y.; Sun, L.; Crooks, R. M. *Macromolecules* **2003**, *36*, 5725.
(45) Engh, R. A.; Huber, R. *Acta Crystallogr.* **1991**, *A47*, 392.
(46) Marsh, R. E.; Donohue, J. *Adv. Protein Chem.* **1967**, *22*, 249.
(47) *Handbook of Chemistry and Physics*, 77th ed.; Lide, D. R., Ed.; CRC Press: Boca Raton, FL, 1997.
(48) Tarazona-Vasquez, F.; Balbuena, P. B. *J. Phys. Chem. B*, **2004**, *108*, 15994.

(49) Hehre, W. J.; Radom, L.; Schleyer, P. v. R.; Pople, J. A. *Ab Initio Molecular Orbital Theory*; John Wiley & Sons: New York, 1986.
(50) Socrates, G. *Infrared and Raman Characteristic Groups. Tables and Charts*, 3rd ed.; John Wiley & Sons: New York, 2001.
(51) Lin-Vien, D.; Colthup, N. B.; Fateley, W. G.; Grasselli, J. G. *The Handbook of Infrared and Raman Characteristic Frequencies of Organic Molecules*; Academic Press: New York, 1991.
(52) Dillon, R. E. A.; Shriver, D. F. *Chem. Mater.* **2001**, *13*, 1369.
(53) Jalkanen, K. J.; Suhai, S. *Chem. Phys.* **1996**, *208*, 81.
(54) Papanek, P.; Fischer, J. E.; Murphy, N. S. *Macromolecules* **2002**, *35*, 4175.
(55) Galabov, B.; Yamaguchi, Y.; Remington, R. B.; Schaefer, H. F, III. *J. Phys. Chem. A* **2002**, *106*, 819.
(56) Scott, A. P.; Radom, L. *J. Phys. Chem.* **1996**, *100*, 16502.
(57) http://srdata.nist.gov/cccbdb/default.htm, 2003.
(58) Halls, M. D.; Velkovski, J.; Schlegel, H. B. *Theor. Chem. Acc.* **2001**, *105*, 413.
(59) Bour, P.; Kubelka, J.; Keiderling, T. A. *Biopolymers* **2000**, *53*.
(60) Grenie, Y.; Avignon, M.; Garribou-Lagrange, C. *J. Mol. Struct.* **1975**, *24*, 293.
(61) Diem, M.; Polavarapu, P. L.; Oboodi, M.; Nafie, L. A. *J. Am. Chem. Soc.* **1982**, *104*, 3329.